Mechanism of *S*-oxygenation by a cysteine dioxygenase model complex

Devesh Kumar[a,b], **G. Narahari Sastry**[a], **David P. Goldberg**[c], and **Sam P. de Visser**[d]

Devesh Kumar: dkclcre@yahoo.com; David P. Goldberg: dpg@jhu.edu; Sam P. de Visser: sam.devisser@manchester.ac.uk

[a]Molecular Modelling Group, Indian Institute of Chemical Technology, Hyderabad 500-607, India

[b]Department of Applied Physics, School for Physical Sciences, Babasaheb Bhimrao Ambedkar University, Vidya Vihar, Rai Bareilly Road, Lucknow 226 025, India

[c]Department of Chemistry, Johns Hopkins University, 3400 N. Charles Street, Baltimore, Maryland 21218, United States

[d]Manchester Interdisciplinary Biocenter and School of Chemical Engineering and Analytical Science, University of Manchester, 131 Princess Street, Manchester M1 7DN, United Kingdom

Abstract

In this work we present the first computational study on a biomimetic cysteine dioxygenase model complex, $[Fe^{II}(LN_3S)]^+$ where LN_3S is a tetradentate ligand with a bis(imino)pyridyl scaffold and a pendant arylthiolate group. The reaction mechanism of sulfur dioxygenation with O_2 was examined by density functional theory (DFT) methods, and compared to results obtained for cysteine dioxygenase. The reaction proceeds via multistate reactivity patterns on competing singlet, triplet and quintet spin state surfaces. The reaction mechanism is analogous to that found for cysteine dioxygenase enzymes [Kumar, D.; Thiel, W.; de Visser, S. P. *J. Am. Chem. Soc.* **2011**, *133*, 3869–3882], hence the computations indicate that this complex can closely mimic the enzymatic process. The catalytic mechanism starts from an iron(III)-superoxo complex and the attack of the terminal oxygen atom of the superoxo group on the sulfur atom of the ligand. Subsequently, the dioxygen bond breaks to form an iron(IV)-oxo complex with a bound sulfenato group. After reorganization the second oxygen atom is transferred to the substrate to give a sulfinic acid product. An alternative mechanism involving the direct attack of dioxygen on the sulfur, without involving any iron-oxygen intermediates, was also examined. Importantly, a significant energetic preference for dioxygen coordinating to the iron center prior to attack at sulfur was discovered and serves to elucidate the function of the metal ion in the reaction process. The computational results are in good agreement with experimental observations, and the differences and similarities of the biomimetic complex and the enzymatic CDO center are highlighted.

Introduction

Biosystems often utilize molecular oxygen on a transition metal center for the biotransformation of substrates. Two characteristic types of transition metal containing oxygenases have been identified, namely the heme and nonheme oxygenases that either

Correspondence to: Devesh Kumar, dkclcre@yahoo.com; David P. Goldberg, dpg@jhu.edu; Sam P. de Visser, sam.devisser@manchester.ac.uk.

transfer one oxygen atom of molecular oxygen to the substrate (monooxygenases) or both oxygen atoms (dioxygenases).[1,2] The heme enzymes include the – well studied – cytochromes P450 enzymes that are monooxygenases and mainly found in the liver, where they catalyze the metabolism of drugs and the biosynthesis of hormones.[1] By contrast, the nonheme iron dioxygenases take part in biocatalysis via oxygen sensing mechanisms, reactions to hypoxia, and DNA and RNA base repair.[2,3] Essentially both classes of oxygenases utilize molecular oxygen on a transition metal center and catalyze an oxygen atom transfer reaction to a substrate, via a substrate hydroxylation (aromatic as well as aliphatic), epoxidation or heteroatom oxidation.

A large group of nonheme iron dioxygenases uses α-ketoglutarate as a co-substrate in the catalytic cycle and, therefore, are called the α-ketoglutarate dependent dioxygenases (αKDD).[4] Structurally, the αKDD have a characteristic active site, where the metal is bound to the protein via a 2-His-1-Asp facial motif.[5] Figure 1(a) shows the active site of substrate bound taurine/α-ketoglutarate dioxygenase (TauD) as taken from the 1OS7 protein databank file (pdb).[6] Substrate taurine is not bound to the iron center directly but in its close vicinity and held in position through a series of hydrogen bonding interactions, for instance, with Arg_{270} and His_{70}. There are a small number of nonheme iron dioxygenases, however, that do not possess the 2-His-1-Asp facial ligand motif, but still catalyze a dioxygenation reaction.[7] One of these enzymes is cysteine dioxygenase (CDO), which is involved in the first step of the catalytic metabolism of cysteine in the body.[8] This is a vital process in our biosystem, since a decline in CDO activity has been associated with neurological disorders and can give rise to diseases such as Alzheimer's and Parkinson's.[9] Despite the important function of CDO in human health, there is surprisingly little known about the mechanism of action of this enzyme. A few single-crystal X-ray diffraction studies have provided important structural information on CDO, and a small amount of spectroscopic measurements on the enzyme have been reported, but thus far there has been no experimental observation of any mechanistic intermediates for the cysteine oxidation carried out by CDO enzymes.[10] In contrast to other nonheme iron dioxygenases, such as TauD, the metal in CDO enzymes is locked in position through bonds with three histidine groups in a facial orientation, see Figure 1(b), as taken from the 2IC1 pdb file.[11] Substrate cysteinate binds as a bidentate ligand to the iron center with the sulfide group *trans* to His_{88} and the amide group trans to His_{140}. The substrate is held in a tight binding pocket and forms a salt bridge between its carboxylic acid group and the side chain of Arg_{60}, but also forms hydrogen bonding interactions with Tyr_{157} and His_{155}. Note also the unusual covalent linkage between Tyr_{157} and Cys_{93}. The sixth ligand site (*trans* to His_{86}) is vacant in the pdb file and reserved for molecular oxygen.

In order to understand the catalytic mechanism of CDO enzymes and the effect of the 3-His ligand system on the reactivity patterns, a series of computational studies were performed.[12] In these calculations it was found that the 3-His ligand system is essential for the dioxygenation process in CDO enzymes, since replacing one of the His ligands by Asp led to weakening of the Fe–S bond and less efficient dioxygenation as compared to wild-type enzyme. In this regard, the influence of a 3-His coordination environment versus the canonical 2-His-1-carboxylate motif is of broad interest.[13] Furthermore, the computational studies gave insight into the mechanism of dioxygen activation by CDO enzymes and the rate-determining step in the reaction mechanism. Scheme 1 summarizes the computationally derived mechanism of dioxygen activation by CDO enzymes. It was shown that the reaction starts from an end-on Fe(III)-superoxo complex (**A**), where the distal oxygen atom (O_d) is hydrogen bonded to the amide group of the cysteinate moiety. This distal oxygen atom, subsequently, attacks the sulfur atom of cysteinate to form a bicyclic ring-structure (**B**) via a rate determining S–O bond formation step. In structure **B** the dioxygen bond is significantly weakened with considerable bond lengthening upon moving from **A** to **B** and breaks via a

small barrier to form an Fe(IV)-oxo bound to cysteine sulfenate (**C**). In structure **C** the sulfur atom is inaccessible to the second oxygen atom, hence an internal rotation takes place to move the sulfenate into the *trans* position in structure **D**. Finally, the second oxygen atom is transferred to the substrate to form the cysteine sulfinic acid product (**E**). Computational modeling at the density functional theory (DFT) and quantum mechanics/molecular mechanics (QM/MM) levels of theory showed the reaction to proceed via multistate reactivity on close lying singlet, triplet and quintet spin states. As such, CDO enzymes follow mechanisms that resemble heme and nonheme dioxygenases which also show two-state-reactivity and multistate reactivity patterns.[14]

Another method to investigate the influence of structure and coordination environment on the mechanism of metalloenzymes is through the synthesis and study of synthetic analogs of their active sites.[15] Some of the best studied of these synthetic models are the iron porphyrins. High-valent iron-oxo porphyrins are postulated as the key intermediates in many heme enzymes, and many synthetic analogs of these intermediates have been generated through the addition of hydrogen peroxide or peracids to a reduced iron porphyrin precursor.[16] Examination of synthetic high-valent iron-oxo porphyrins has provided many important insights regarding structure and function. For example, the binding of variable axial ligands to iron(IV)-oxo porphyrin complexes helped establish a *trans* effect on reactivity patterns as well as a *trans* influence on spectroscopic parameters.[17] Reactivity patterns of systems with different axial ligands (neutral versus anionic) showed changes in the regioselectivity of aromatic versus aliphatic hydroxylation, reactivity patterns of *cis* versus *trans* olefins, and kinetic isotope effects for hydrogen atom abstraction reactions.[18] A *trans* influence of thiolate donors on nonheme Fe^{III}-OOR model complexes has also been described, providing evidence for a weakening of the Fe–O bond upon increasing thiolate electron donation.[19] These findings suggested a role for the unusual *trans*-ligated Cys donor in the nonheme iron enzyme superoxide reductase.[20] These previous studies highlight the role that model complexes play in defining the fundamental influences of biomimetic ligands on the properties of biologically relevant metal centers.

Some of the first functional synthetic models of the active site of CDO have been reported by one of us, including the iron(II) model complex displayed in Scheme 2.[21] The CDO biomimetic model contains a bis(imino)pyridine ligand with a pendant thiolate group (LN_3S), which binds iron as a tetradentate ligand through the three nitrogen atoms and the thiolate group. Reaction of this complex with excess dioxygen affords a product in which the thiolate donor has been oxygenated to give a terminal $-SO_3^-$ (sulfonato) group. Studies involving the use of ^{18}O isotopically-labeled dioxygen revealed that all 3 oxygen atoms of the sulfonato product originated from O_2 as opposed to H_2O, and mixed $^{18}O_2/^{16}O_2$ experiments indicated that two oxygens in the $-SO_3^-$ group derived from one molecule of O_2. Thus a reasonable mechanistic hypothesis for *S*-oxygenation in the model complex involved an initial step similar to the enzyme involving dioxygenation of the sulfur atom, followed by a second monoxygenation step. However, what the mechanism of dioxygen activation is, and whether it is analogous to CDO enzymes, remain open questions and ripe for computational analysis.

The selective *S*-oxygenation of sulfur-bound metal complexes with O_2 as oxidant is a relatively rare process, although several biomimetic Ni(II) complexes were found to perform this process efficiently.[22] There are also a few examples of Ru(II)-, and Fe(III)-thiolates reacting with O_2 to give *S*-oxygenated products.[23,24] Although not much mechanistic information is available for the former complexes, it is possible that these complexes proceed through a mechanism similar to that postulated for the Ni(II)-thiolates, in which the coordinated S-atom functions as a nucleophile for direct attack on O_2. In this scenario *S*-oxygenation does not involve O_2 activation at the metal in a redox process. Alternatively, a

related possible mechanism for *S*-oxygenation could be similar to the mechanism proposed for extradiol dioxygenases, where the nonheme iron center serves to activate the bound substrate toward a coordinated O_2 molecule, but there are no formal redox state changes at Fe to activate O_2.[25] Thus, one or more of these mechanisms are possible for both CDO as well as the synthetic analog in Scheme 2. The question of whether an Fe(III)-superoxo species is formed prior to *S*-oxygenation is a question of fundamental importance to both CDO and related model complexes.

To establish a reaction mechanism of dioxygen transfer to the iron(II) model complex in Scheme 2, as well as the *S*-oxygenation process of the LN$_3$S ligand, we decided to do a series of density functional theory calculations and specifically focus on the difference between a reaction starting from an iron(III)-superoxo complex and one where molecular oxygen directly reacts with the thiolate ligand. We then compare the obtained results with those recently published on CDO enzymes, nonheme iron dioxygenases and biomimetic model complexes.

Methods

Following previous experience in the field,[26] we use density functional theory studies on the biomimetic model of CDO as displayed in Scheme 2. The calculations were performed with the *Jaguar* and *Gaussian* program packages.[27] The unrestricted hybrid density functional method B3LYP was selected,[28] since previous studies of ours showed that this method gives rate constants within $2 - 3$ kcal mol^{-1} from experiment.[29] Moreover, QM/MM studies using a series of density functional methods describing the QM region showed that B3LYP gives results close in energy to other methods tested.[12c] Furthermore, the use of similar methods and techniques as those in ref 14 enables us to make a direct comparison between the performance of the biomimetic model studied here with the enzymatic system.

Initial geometry optimizations were done with a Los Alamos-type LACVP basis set on iron that contains a core potential, whereas the rest of the atoms are described with 6-31G, basis set BS1.[30] Subsequent single point calculations utilize the LACV3P+ basis set on iron that includes a core potential and 6-311+G* on the rest of the atoms; basis set BS2. Previous studies of ours showed that this combination of methods gives reliable geometries and energetics that are within a few tenths of a kcal mol^{-1} from those obtained after a full geometry optimization at UB3LYP/BS2.[31] Relative energies reported here were obtained with basis set BS2 and corrected for zero-point energy from the Gaussian frequency calculations. Free energies contain UB3LYP/BS1 zero-point, thermal and entropy calculated corrections at 298 K and use UB3LYP/BS2 energies.

All structures were subjected to a full geometry optimization without constraints and followed by an analytical frequency calculation at the same level of theory. To establish a reaction mechanism between the various local minima, first we performed extensive geometry scans whereby one degree of freedom (the reaction coordinate) was frozen and all other degrees of freedom fully optimized. These geometry scans established pathways between the various local minima and the maxima of these scans were used as starting point for the transition state geometry searches. The effect of the environment was tested through single point calculations in a dielectric constant of $\varepsilon = 5.7$ mimicking a chlorobenzene solution using the Poisson-Boltzmann solvation model as implemented in *Jaguar* 7.7.

Results and Discussion

Iron(III)-superoxo species in biomimetic and enzymatic CDO complexes

Following previous experience in the field[12] we started the dioxygenation studies from an iron(III)-superoxo complex shown in Figure 2. This complex was generated from the crystal structure coordinates of $[Fe^{II}(LN_3S)(OTf)]$ reported in Ref 21a, whereby the *iso*-propyl groups were replaced by hydrogen atoms to help facilitate the computations. Mass spectrometry analysis of the product distributions identified $[Fe^{II}(LN_3SO_2)]^+$ products although it reacted over time to the triply oxygenated product probably in reaction with a second molecule of O_2. The CDO enzymes contain an active site, where there is a neutral histidine group *trans* to the dioxygen binding site on the metal and, therefore, we decided to remove the triflate anion and replaced it by molecular oxygen. Computational studies of the axial ligand effect of hydrogen atom abstraction versus aromatic hydroxylation by iron(IV)-oxo complexes with axial acetonitrile versus chloride showed dramatic differences due to the charge of the axial ligand, i.e. neutral versus anionic axial ligands.[32] With triflate removed our computational model shows close similarity to the active site of CDO enzymes. These coordinates were optimized and resulted in a structure that showed little deviation from the crystal structure. Optimized geometries of the Fe(III)-superoxo complexes (^{1,3,5}**A**) in the lowest lying singlet, triplet and quintet spin states are shown in Figure 2. The structures are characteristic of an iron(III)-superoxo complex where the superoxo group is bound in an end-on fashion. The bond lengths obtained are similar to those calculated for iron(III)-superoxo complexes in heme and nonheme environments.[14a,33] Crystallographic data on enzymatic end-on ferric-superoxo complexes gave Fe–O and O–O distances of approximately 2.06 and 1.22 Å, respectively, which are values close to those given in Figure 2.[34] Relative energies give close lying singlet, triplet and quintet spin state structures, where the spin state ordering varies with the method chosen. Gas-phase relative energies give the singlet spin state below the quintet by about 2.1 kcal mol^{-1}, but free energy and solvent corrections reverse this and make the quintet spin state the ground state by 1.2 kcal mol^{-1}. No experimental data are available on the iron(III)-superoxo complex, however the Fe(II) complex without O_2 is in a quintet spin state,[21a] which makes it likely that the Fe(III)-superoxo complex should be in a high-spin state too. Nevertheless, it is clear that the iron(III)-superoxo species exists in close-lying spin states and, therefore, will react via multistate reactivity patterns.

The spin-state ordering and relative energies for ^{1,3,5}**A** found here is considerably different from that reported before for the CDO enzyme active site derived from either DFT methods or QM/MM. To understand these differences, let us analyze the orbital differences in more detail; Figure 3 shows the high-lying occupied and low-lying virtual orbitals for ^{5}**A** as an example of the orbital shapes. The other spin states have similar molecular orbitals but the only difference is their occupation. The molecular orbitals displayed in Figure 3 originate from the metal $3d$ orbitals and the interactions they undergo with the $2p$ orbitals on the superoxo group and the nitrogen and sulfur atoms of the LN_3S ligand and consist of six π^* type and three σ^* type orbitals, which we label as $\pi^*_1 - \pi^*_6$ and $\sigma^*_1 - \sigma^*_3$. The lowest lying molecular orbital with metal $3d$ contribution is the doubly occupied π^*_1 (π^*_{xy}) orbital that is comprised of the $3d_{xy}$ orbital on Fe in interaction with a $3p$ orbital on sulfur. Another doubly occupied orbital is the $\sigma_{z2} + \pi^*_{OO,yz}$ mixed orbital that has the bonding combination of the out-of-plane $3d_{z2}$ orbital with the antibonding π^*_{OO} orbital along the yz-axis; σ^*_1. The antibonding combination of this orbital, labeled as σ^*_2, is singly occupied and has a dominant $3d_{z2}$ component on the metal. The metal $3d_{xz}$ and $3d_{yz}$ atomic orbitals form bonding and antibonding combinations with the $\pi^*_{OO,xz}$ and $\pi^*_{OO,yz}$ orbitals on the superoxo group, respectively. Along the yz-axis there is one pair of $\pi^*_{yz} \pm \pi^*_{OO,yz}$; the positive combination (π^*_3) is singly occupied and the negative one (π^*_5) is a virtual orbital. By contrast, along the xz-axis there are three possible combinations, namely bonding (π^*_2),

nonbonding ($\pi*_4$) and antibonding ($\pi*_6$). The bonding combination ($\pi*_{xz} + \pi*_{OO,xz}$) and the nonbonding $\pi*_{OO,xz}$ orbitals are singly occupied in the quintet spin state, while the antibonding $\pi*_{xz} - \pi*_{OO,xz}$ is virtual. Finally, high-lying and virtual is the $\sigma*_{x2-y2}$ orbital for the antibonding interactions of the metal with the four ligand atoms in the xy-plane ($\sigma*_3$). These set of orbitals have an occupation of $\pi*_1^2 \sigma*_1^2 \sigma*_2^1 \pi*_2^1 \pi*_3^1 \pi*_4^1$ for ^{5}**A**, whereas ^{3}**A** has an occupation of $\pi*_1^2 \sigma*_1^2 \pi*_2^2 \pi*_3^1 \pi*_4^1$ and ^{1}**A** an occupation of $\pi*_1^2 \sigma*_1^2 \sigma*_2^1 \pi*_2^\downarrow \pi*_3^\uparrow \pi*_4^\downarrow$. Double occupation of $\pi*_2$ in the triplet spin state leads to enhanced bonding between the metal and oxygen atom and considerable shortening of the Fe–O bond with respect to the singlet and quintet spin state structures.

As follows from the orbital diagrams in Figure 3, the $3d_{xz}$ and $3d_{yz}$ atomic orbitals on Fe mix with orbitals on the π-system on the LN$_3$S ligand and the $\pi*_{OO}$ orbitals to create a series of mixed orbitals, e.g. $\pi*_2 - \pi*_6$. As a consequence of this, the orbital energy levels in our biomimetic CDO model are very different from those found for the enzymatic system. Note, for instance, that in CDO enzymes the ligands in the xy-plane are histidine amino acids, but their aromatic rings are not aligned with the xy-plane but are perpendicular to it. Consequently, the iron(III)-superoxo species in CDO enzymes has a singlet spin ground state that is well separated from the quintet spin state by more than 10 kcal mol^{-1},[12c] whereas in the biomimetic system the singlet and quintet spin states are close in energy. This will also affect the subsequent oxygen atom transfer processes as will be shown later.

Reaction mechanism of *S*-oxygenation

Next, we investigated the dioxygenation of the thiolate group of the LN$_3$S ligand according to the mechanism found for CDO enzymes (Scheme 1), and the results are shown in Figure 4. The reaction starts from the iron(III)-superoxo complexes (^{1,3,5}**A**) with the attack of the distal oxygen atom on the sulfur atom to form a bicyclic ring-structure (^{1,3,5}**B**) via an S–O bond formation barrier (^{1,3,5}**TS1**). In the bicyclic structure the dioxygen bond is weakened and breaks via a barrier ^{1,3,5}**TS2** to form a sulfenate bound to an iron(IV)-oxo moiety (^{1,3,5}**C**). Thereafter, the sulfenate group undergoes an internal rotation to form the isomeric structure ^{1,3,5}**D** via a barrier ^{1,3,5}**TS3**. In a final step the second oxygen atom is transferred via a transition state ^{1,3,5}**TS4** to give the sulfinic acid product complex (^{1,3,5}**E**).

Although the singlet spin state is low in energy for the iron(III)-superoxo complex, it actually plays little effect on the reaction mechanism due to the fact that ^{1}**TS1** and ^{1}**TS2** barriers are very high in energy, i.e. well over 25 kcal mol^{-1}. As a matter of fact the complete singlet spin potential energy surface beyond ^{1}**TS1** is at least 10 kcal mol^{-1} above the lowest lying spin state surface, which means that the singlet spin state will contribute very little to the overall reaction mechanism.

At the free energy level, the quintet spin iron(III)-superoxo complex is the ground state. Similar to gas-phase DFT studies on CDO enzymes,[12a] the S–O bond formation barrier (**TS1**) is also the lowest on the quintet spin state surface. As follows from Figure 4 at the free energy level, the mechanism starting from the iron(III)-superoxo complex until the iron(IV)-sulfenate complex will take place on a dominant quintet spin state surface only. The nearest other spin state is at least 7 kcal mol^{-1} higher in energy in the mechanism leading up to the iron(IV)-sulfenate complex (**C**), but the triplet and quintet spin states converge in this point and ^{3,5}**C** are energetically close with a small preference for the triplet spin state. As shown before, biomimetic nonheme iron(IV)-oxo complexes have a triplet spin ground state,[35] which contrasts the situation for enzymatic nonheme iron(IV)-oxo complexes that have been characterized as high-spin states.[36] Computational studies explained this difference through differences in orbital interactions of the $\pi*_{xy}$ and $\sigma*_{x2-y2}$ molecular orbitals that change their relative energy and thereby affect the triplet-quintet energy splitting and ordering.[37]

The rotational barrier from ^{3,5}C to reach ^{3,5}D, i.e. ^{3,5}TS3, is relatively small; therefore, the system will interconvert to **D** rapidly. The final oxygen atom transfer via barrier **TS4** is large on the quintet spin state but much smaller on the triplet spin state surface, although it is not the highest barrier. The rate determining step in the CDO biomimetic reaction mechanism is the process passing **TS2**, which has a free energy of activation of 22 kcal mol^{-1} relative to reactant complexes on the quintet spin state surface. This contrasts the mechanisms found for CDO enzymes where the step passing **TS1** was found to be rate determining.[12]

Optimized geometries of the local minima along the reaction mechanism are displayed in Figure 5, while the optimized transition state structures are given in Figure 6. Optimized geometries are in line with previous DFT and QM/MM studies on the catalytic mechanism of dioxygen transfer from the iron center in the enzyme to cysteinate substrate. As discussed above the reaction starts from an iron(III)-superoxo structure that is in close-lying singlet and quintet spin states with the latter slightly lower in energy. Attack of the terminal oxygen atom of the superoxo group on the thiolate sulfur creates an O–S bond and forms the ring-structure **B**. In these structures the superoxo O–O bond is weakened, elongating from 1.286 – 1.328 Å in ^{1,3,5}A to a distance near 1.5 Å in ^{1,3,5}B, which is consistent with a formal single bond. At the same time, the Fe–S bond is weakened from 2.248 Å in ^{1,3,5}A to 2.359 Å in ^{1}B and 2.613 Å in ^{5}B. In the quintet spin state there is also a certain degree of bond lengthening between the metal and the three bound nitrogen atoms. Because of the weakening of the superoxide O–O bond, it costs relatively little extra energy to break it and form the iron(IV)-oxo with a sulfenate ligand, structure **C**. In this structure the iron-sulfur bond is weakened further and, in particular, in the quintet spin state it has dissociated (Fe–S distance of 3.235 Å in ^{5}C). Subsequently, the oxygen atom of the sulfenate binds to the metal to form structures **D** followed by the final oxygen atom transfer to form products, **E**.

The transition state structures are analogous to those found for CDO enzymes.[12] The O–O bond lengthens in **TS1** to a value ranging from 1.421 − 1.432 Å. The imaginary frequency in the transition state represents the S–O stretch vibration and is characteristic for an S–O bond formation step. In **TS2** the O–O bond is further elongated and the imaginary frequency shows an O–O stretch vibration that represents the O–O dissociation step in the reaction mechanism. Note also that some saddling in the LN$_3$S ligand structure has taken place in **TS1** although the saddling is lost in **TS2** and onwards. If we define a dihedral angle through the three nitrogen atoms of the LN$_3$S ring and the *para*-carbon atom of the R group (C1-N1-N3-N2) in Figure 6, we find a saddling of −165.7° in ^{3}TS1, −169.9° in ^{1}TS1 and −175.3° in ^{5}TS1, which implicates deviations from planarity of 14.3, 10.1 and 4.7°, respectively. Thus, the orbital occupation in the triplet spin state with shortened Fe–O distances causes structural distortion and saddling.

Thus the calculations predict that the iron center of the model complex functions to coordinate and activate O$_2$ toward O–O bond cleavage and oxygen transfer to the thiolate group. They also show that O-atom transfer to the thiolate S atom is relatively facile, providing a smooth mechanism for *S*-oxygenation. The computed mechanism predicts a dioxygenase type mechanism wherein two oxygen atoms in the final product are derived from one molecule of O$_2$, which is nicely consistent with experimental evidence from ^{18}O$_2$ isotope-labeling mass spectrometry studies. It may further be anticipated that the third oxygen atom transfer to form the −SO$_3$ complex will proceed after binding a second molecule of molecular oxygen and a subsequent monoxygenation step of the sulfinic acid intermediate.

Comparison between CDO enzyme and the biomimetic model

Unfortunately no experimental data on wild-type CDO or biomimetic model complexes exists after dioxygen binding, so that a comparison of the obtained results with experiment is

not possible, therefore we will compare the work with previous computations in the field. At a first glance, the obtained results of the biomimetic model seem to give considerable differences as compared to DFT and QM/MM studies on the CDO enzyme, which we will compare in detail in the following. Table 1 gives relative energies of the dioxygen transfer process in $[Fe^{III}(LN_3S)O_2]^+$ as described in this work as compared to two published set of calculations on CDO enzymes: the first uses a DFT model complex of 81 atoms from Ref 12a, whereas the second is the result of the full QM/MM calculation reported in Ref 12c. The calculations on $[Fe^{III}(LN_3S)O_2]^+$ and the CDO model complex use the same methods and techniques and energetics including ZPE and solvent corrections. As can be seen from Table 1, the obtained potential energy landscape for these two chemical systems is very similar with some minor deviations we will discuss below. Based on the energetic profile, therefore, it appears that the $[Fe^{III}(LN_3S)O_2]^+$ is a good model of CDO enzymes. At this level of theory the singlet spin state is the ground state of the iron-superoxo complex, but as discussed above at the free energy level the quintet spin state becomes the ground state. This lowering of the quintet spin state surface in the Fe(III)-superoxo reactant has further consequences for the overall kinetics of the reaction. Thus, in the enzymatic system using DFT model complexes a rate determining ⁵**TS1** barrier was found and all subsequent barriers were found to be smaller than their precursors, i.e. ⁵**TS1** > ⁵**TS2** > ⁵**TS3** > ⁵**TS4**. Due to lowering of the energy of ⁵**A** in the biomimetic model, as a consequence also ⁵**TS1** is lowered in energy. Accordingly, the biomimetic CDO model complex has a rate determining step via ⁵**TS2**, while the enzymatic DFT model has a rate determining ⁵**TS1** step. These differences in barriers should lead to different kinetic behavior for these two systems. The rest of the mechanism is very much alike for the biomimetic and CDO model complexes apart from a relatively high ⁵**TS4** barrier in the biomimetic model system.

On the singlet spin potential energy surface, the deviation between the biomimetic and enzymatic model complexes is less than 5.7 kcal mol⁻¹ for all structures. This is also the case for the triplet spin state surface until ³**TS3**, beyond this point significant deviations occur between the enzymatic and biomimetic model complexes and the biomimetic ³**D** and ³**TS4** structures are stabilized considerably. It should be noted, however, that the actual barrier from ³**D** to ³**TS4** is similar in energy to that found in the enzymatic calculations. Hence this only affects the driving force for ³**D** to ³**E** but not the kinetics.

The differences between the QM/MM studies on CDO enzymes and the biomimetic model system are more pronounced and require further elaboration. As mentioned above the quintet spin state of the iron(III)-superoxo structure is significantly higher in energy in the QM/MM studies than in either DFT model complexes. This is not only due to destabilization of the quintet but also as a result of stabilization of the singlet spin state surface. The latter further leads to a low ¹**TS1** barrier that is competitive with the quintet spin barrier. Accordingly, in the QM/MM calculations multistate reactivity patterns on competing singlet, triplet and quintet spin state surfaces are found, where the reaction starts in ¹**A** and proceeds via ¹**TS1** to ¹**B** or via a spin-state crossing to ³**B**. Depending on the lifetime of this intermediate a further electron transfer process can lead to a second spin-state crossing to the quintet spin state. However, the **TS2** barriers are low and the most stable **C** structure is in the triplet spin state. The ⁵**TS3** and ⁵**TS4** barriers are considerably lower in energy than ³**TS3** and ³**TS4**, so that it is likely that the spin-state crossing to the quintet spin state will take place in or around **TS3/TS4** in the reaction mechanism to give quintet spin state products. This multistate reactivity mechanism has a rate determining ¹**TS1** barrier and will contain two spin state crossings, one from singlet to triplet and another from triplet to quintet.

Despite the differences in relative energies of **A** and **TS1** in the biomimetic model complex as compared to the QM/MM calculations on the enzyme, in the ring-structures all energies

converge to very similar values. The dioxygen bond breaking step has small barriers on each spin state surface in the QM/MM calculations, but much larger barriers are found in the biomimetic model system, where this step even is rate determining. Presumably the hydrogen bonding and polar interactions in the substrate binding pocket of the enzyme facilitate smooth dioxygen bond breakage and the formation of the sulfenate intermediate. These interactions are absent in the biomimetic model and hence the dioxygen bond breaking barriers are higher.

Direct oxygen atom transfer to sulfur without metal assistance

One of the key remaining questions in CDO catalysis relates to the involvement of the transition metal in the conversion of cysteine into cysteine sulfinic acid products. Thus, does the metal just hold the substrate into position, while being electronically inactive, or does it play an active role by donating electrons into the process. To address this question, we did a subsequent experiment, where molecular oxygen is not bound to the transition metal at the start of the reaction but approaches the thiolate-bound $[Fe^{II}(LN_3S)]^+$ from a large (> 6 Å) distance. The obtained geometry scan is given in Figure 7 for the singlet, triplet and quintet spin states. In these studies we investigate the direct attack of molecular oxygen on the thiolate group without binding the metal first. To this end, the dioxygen starts at a large distance from the metal and sulfur centers and in stepwise (full geometry) optimizations, we move the dioxygen moiety closer to the sulfur atom by fixing the S–O distance while optimizing all other degrees of freedom.

During the geometry scan, however, prior to the formation of an actual O–S bond, the dioxygen molecule approaches the metal center and binds in the usual Fe(III)-superoxo form, thereby stabilizing our chemical system with a couple of kcal mol^{-1}. This happens on all three spin state surfaces. As a consequence, the minimum points in the scans shown in Figure 7, labeled as ^{1,3,5}**A'**, geometrically resemble the Fe(III)-superoxo optimized geometries discussed above in Figure 5. Consequently, approach of molecular oxygen onto the sulfur atom bound to a metal center will first lead to a stable metal-superoxo complex. These results predict that direct attack of the thiolate group by molecular oxygen should be high in energy.

From the local minima in Figure 7, we continued the geometry scans for the S–O bond formation. The reaction proceeds in a similar way as shown above in Figure 4 with similar barrier heights and rate constants. Shortening of the S–O bond further indeed gives transition state structures similar to those reported above that started from ^{1,3,5}**A** and lead to analogous ring-structure complexes. Therefore, direct attack of dioxygen on the thiolate group is unlikely to take place and binding of molecular oxygen will give a stable iron(III)-superoxo complex that is able to transfer both oxygen atoms to a sulfur containing substrate located in the *cis*-position.

In summary, it is essential for the reaction that molecular oxygen binds the metal center first, since it leads to stable open-shell spin states as shown by the orbital diagram in Figure 2. Furthermore, it enables a stepwise oxygen atom transfer mechanism as described in Scheme 1, where the first step is focused on O–O bond weakening and breaking. The results on the model complex suggest that the iron center in CDO has dual functions in the *S*-oxygenation mechanism. Firstly, it holds the substrate into a tight but specific orientation. Secondly, it binds molecular oxygen, whereby the electrons are redistributed in metal-superoxo type orbitals that enable efficient oxygen atom transfer mechanisms.

Conclusions

Density functional theory calculations have been performed on the mechanism of LN_3S dioxygenation on an iron center. This reaction mimics that found for CDO enzymes and gives fundamental insight into the metal ligand system on reactivity. We investigated two reaction mechanisms: one involves binding of dioxygen to iron, while the other involves a direct attack of dioxygen on the sulfur atom. The calculations show that the binding of O_2 to Fe is energetically favorable, and during the geometry scan for dioxygen approach to the sulfur atom the O_2 molecule binds the iron atom immediately. These calculations indicate that the formation of the iron(III)-superoxo complex is thermodynamically driven and will lead to the reaction mechanism analogous to the one calculated for CDO enzymes. A detailed structural, thermodynamic and kinetic comparison of the CDO mimic and the enzyme gives close similarities between the biomimetic model system and wild-type enzyme and supports the assignment of iron(II)(LN_3S) as a CDO mimic.

Supplementary Material

Refer to Web version on PubMed Central for supplementary material.

Acknowledgments

References

1. (a) Sono M, Roach MP, Coulter ED, Dawson JH. Chem Rev. 1996; 96:2841–2888. [PubMed: 11848843] (b) Kadish, KM.; Smith, KM.; Guilard, R., editors. The Porphyrin Handbook. Vol. 4. Academic Press; San Diego, CA: 2000. (c) Guengerich FP. Chem Res Toxicol. 2001; 14:611–650. [PubMed: 11409933] (d) Groves JT. Proc Natl Acad Sci USA. 2003; 100:3569–3574. [PubMed: 12655056] (e) Ortiz de Montellano, PR., editor. Cytochrome P450: Structure, Mechanism and Biochemistry. 3. Kluwer Academic /Plenum Publishers; New York: 2004. (f) Munro AW, Girvan HM, McLean KJ. Nat Prod Rep. 2007; 24:585–609. [PubMed: 17534532] (g) Shaik S, Hirao H, Kumar D. Nat Prod Rep. 2007; 24:533–552. [PubMed: 17534529] (h) Meunier B, de Visser SP, Shaik S. Chem Rev. 2004; 104:3947–3980. [PubMed: 15352783]

2. (a) Solomon EI, Brunold TC, Davis MI, Kemsley JN, Lee S-K, Lehnert N, Neese F, Skulan AJ, Yang Y-S, Zhou J. Chem Rev. 2000; 100:235–349. [PubMed: 11749238] (b) Bugg TDH. Curr Opin Chem Biol. 2001; 5:550–555. [PubMed: 11578928] (c) Costas M, Mehn MP, Jensen MP, Que L Jr. Chem Rev. 2004; 104:939–986. [PubMed: 14871146] (d) Bruijnincx PCA, van Koten G, Klein Gebbink RJM. Chem Soc Rev. 2008; 37:2716–2744. [PubMed: 19020684] (e) Bugg TDH, Ramaswamy S. Curr Opin Chem Biol. 2008; 12:134–140. [PubMed: 18249197] (f) de Visser, SP.; Kumar, D., editors. Iron-containing enzymes: Versatile catalysts of hydroxylation reactions in nature. RSC Publishing; Cambridge (UK): 2011.

3. (a) Trewick, SC.; Henshaw, TF.; Hausinger, RP.; Lindahl, T.; Sedgwick, B. Nature. Vol. 419. 2002. p. 174-178.(b) Falnes PØ, Johansen RF, Seeberg E. Nature. 2002; 419:178–182. [PubMed: 12226668] (c) Mishina Y, Duguid EM, He C. Chem Rev. 2006; 106:215–232. [PubMed: 16464003]

4. (a) Krebs C, Fujimori DG, Walsh CT, Bollinger JM Jr. Acc Chem Res. 2007; 40:484–492. [PubMed: 17542550] (b) Schofield CJ, Zhang Z. Curr Opin Chem Biol. 1999; 9:722–731.(c) Bugg TDH. Tetrahedron. 2003; 59:7075–7101.

5. Que L Jr. Nat Struct Biol. 2000; 7:182–184. [PubMed: 10700270]

6. O'Brien JR, Schuller DJ, Yang VS, Dillard BD, Lanzilotta WN. Biochemistry. 2003; 42:5547–5554. [PubMed: 12741810]

7. Straganz GD, Nidetzky B. Chem Bio Chem. 2006; 7:1536–1548.

8. (a) Stipanuk MH. Annu Rev Nutr. 2004; 24:539–577. [PubMed: 15189131] (b) Joseph CA, Maroney MJ. Chem Commun. 2007; (32):3338–3349.(c) Stipanuk MH, Ueki I, Dominy JE Jr, Simmons CR, Hirschberger LL. Amino Acids. 2009; 37:55–63. [PubMed: 19011731]

9. (a) Perry TL, Norman MG, Yong VW, Whiting S, Crichton JU, Hansen S, Kish S. J Ann Neurol. 1985; 18:482–489.(b) Heafield MT, Fearn S, Steventon GB, Waring RH, Williams AC, Sturman SG. Neurosci Lett. 1990; 110:216–220. [PubMed: 2325885]

10. (a) McCoy JG, Bailey LJ, Bitto E, Bingman CA, Aceti DJ, Fox BG, Phillips GN Jr. Proc Natl Acad Sci USA. 2006; 103:3084–3089. [PubMed: 16492780] (b) Simmons CR, Liu Q, Huang Q, Hao Q, Begley TP, Karplus PA, Stipanuk MH. J Biol Chem. 2006; 281:18723–18733. [PubMed: 16611640] (c) Dominy JE Jr, Simmons CR, Karplus PA, Gehring AM, Stipanuk MH. J Bacteriol. 2006; 188:5561–5569. [PubMed: 16855246] (d) Pierce BD, Gardner JD, Bailey LJ, Brunold TC, Fox BG. Biochemistry. 2007; 46:8569–8578. [PubMed: 17602574] (e) Dominy JE Jr, Hwang J, Guo S, Hirschberger LL, Zhang S, Stipanuk MH. J Biol Chem. 2008; 283:12188–12201. [PubMed: 18308719] (f) Kleffmann T, Jongkees SAK, Fairweather G, Wilbanks SM, Jameson GNL. J Biol Inorg Chem. 2009; 14:913–921. [PubMed: 19373496] (g) Gardner JD, Pierce BS, Fox BG, Brunold TC. Biochemistry. 2010; 49:6033–6041. [PubMed: 20397631]

11. Ye S, Wu X, Wei L, Tang D, Sun P, Bartlam M, Rao Z. J Biol Chem. 2007; 282:3391–3402. [PubMed: 17135237]

12. (a) Aluri S, de Visser SP. J Am Chem Soc. 2007; 129:14846–14847. [PubMed: 17994747] (b) de Visser SP, Straganz GD. J Phys Chem A. 2009; 113:1835–1846. [PubMed: 19199799] (c) Kumar D, Thiel W, de Visser SP. J Am Chem Soc. 2011; 133:3869–3882. [PubMed: 21344861] (d) de Visser SP. Coord Chem Rev. 2009; 253:754–768.

13. Diebold AR, Neidig ML, Moran GR, Straganz GD, Solomon EI. Biochemistry. 2010; 49:6945–6952. [PubMed: 20695531]

14. (a) Shaik S, Kumar D, deVisser SP, Altun A, Thiel W. Chem Rev. 2005; 105:2279–2328. [PubMed: 15941215] (b) Hirao H, Kumar D, Que L Jr, Shaik S. J Am Chem Soc. 2006; 128:8590–8606. [PubMed: 16802826]

15. (a) Kryatov SV, Rybak-Akimova EV, Schindler S. Chem Rev. 2005; 105:2175–2226. [PubMed: 15941212] (b) Abu-Omar MM, Loaiza A, Hontzeas N. Chem Rev. 2005; 105:2227–2252. [PubMed: 15941213] (c) Nam W. Acc Chem Res. 2007; 40:522–531. [PubMed: 17469792]

16. (a) Groves, JT. Cytochrome P450: Structure, Mechanism and Biochemistry. 3. Ortiz de Montellano, PR., editor. Vol. Chapter 1. Kluwer Academic/Plenum Publishers; New York: 2005. p. 1-44.(b) de Visser, SP.; Nam, W. Handbook of Porphyrin Science. Kadish, KM.; Smith, KM.; Guilard, R., editors. Vol. Chapter 44. World Scientific Publishing Co.; New Jersey: 2010. p. 85-140.

17. (a) Gross Z, Nimri S. Inorg Chem. 1994; 33:1731–1732.(b) Gross Z. J Biol Inorg Chem. 1996; 1:368–371.(c) Czarnecki K, Nimri S, Gross Z, Proniewicz LM, Kincaid JR. J Am Chem Soc. 1996; 118:2929–2935.

18. (a) Sastri CV, Park MJ, Ohta T, Jackson TA, Stubna A, Seo MS, Lee J, Kim J, Kitagawa T, Münck E, Que L Jr, Nam W. J Am Chem Soc. 2005; 127:12494–12495. [PubMed: 16144389] (b) Song WJ, Ryu YO, Song R, Nam W. J Biol Inorg Chem. 2005; 10:294–304. [PubMed: 15827730] (c) Sastri CV, Lee J, Oh K, Lee YJ, Lee J, Jackson TA, Ray K, Hirao H, Shin W, Halfen JA, Kim J, Que L Jr, Shaik S, Nam W. Proc Natl Acad Sci USA. 2007; 104:19181–19186. [PubMed: 18048327] (d) Prokop KA, de Visser SP, Goldberg DP. Angew Chem Int Ed. 2010; 49:5091–5095.(e) Prokop KA, Neu HM, de Visser SP, Goldberg DP. J Am Chem Soc. 2011; 133:15874–15877. [PubMed: 21888343]

19. (a) Namuswe F, Hayashi T, Jiang Y, Kasper GD, Sarjeant AAN, Moënne-Loccoz P, Goldberg DP. J Am Chem Soc. 2010; 132:157–167. [PubMed: 20000711] (b) Namuswe F, Kasper GD, Sarjeant AAN, Hayashi T, Krest CM, Green MT, Moënne-Loccoz P, Goldberg DP. J Am Chem Soc. 2008; 130:14189–14200. [PubMed: 18837497] (c) Krishnamurthy D, Kasper GD, Namuswe F, Kerber WD, Sarjeant AAN, Moënne-Loccoz P, Goldberg DP. J Am Chem Soc. 2006; 128:14222–14223. [PubMed: 17076472]

20. (a) Kurtz DM Jr. J Inorg Biochem. 2006; 100:679–693. [PubMed: 16504301] (b) Dey A, Jenney FE, Adams MWW, Johnson MK, Hodgson KO, Hedman B, Solomon EI. J Am Chem Soc. 2007;

129:12418–12431. [PubMed: 17887751] (c) Brines LM, Kovacs JA. Eur J Inorg Chem. 2007:29–38.

21. (a) Jiang Y, Widger LR, Kasper GD, Siegler MA, Goldberg DP. J Am Chem Soc. 2010; 132:12214–12215. [PubMed: 20712312] (b) Badlei YM, Siegler MA, Goldberg DP. J Am Chem Soc. 2011; 133:1274–1277. [PubMed: 21207980]

22. (a) Farmer PJ, Solouki T, Mills DK, Soma T, Russell DH, Reibenspies JH, Darensbourg MY. J Am Chem Soc. 1992; 114:4601–4605.(b) Grapperhaus CA, Darensbourg MY. Acc Chem Res. 1998; 31:451–459.(c) Maroney MJ, Choudhury SB, Bryngelson PA, Mirza SA, Sherrod MJ. Inorg Chem. 1996; 35:1073–1076. [PubMed: 11666287] (d) Mirza SA, Pressler MA, Kumar M, Day RO, Maroney MJ. Inorg Chem. 1993; 32:977–987.

23. (a) Masitas CA, Mashuta MS, Grapperhaus CA. Inorg Chem. 2010; 49:5344–5346. [PubMed: 20486695] (b) Masitas CA, Kumar M, Mashuta MS, Kozlowski PM, Grapperhaus CA. Inorg Chem. 2010; 49:10875–10881. [PubMed: 20973591]

24. (a) Heinrich L, Li Y, Vaissermann J, Chottard G, Chottard JC. Angew Chem Int. 1999; 38:3526–3528.(b) Noveron JC, Olmstead MM, Mascharak PK. J Am Chem Soc. 2001; 123:3247–3259. [PubMed: 11457060] (c) Galardon E, Giorgi M, Artaud I. Chem Commun. 2004:286–287.(d) O'Toole MG, Kreso M, Kozlowski PM, Mashuta MS, Grapperhaus C. J Biol Inorg Chem. 2008; 13:1219–1230. [PubMed: 18633652]

25. Lipscomb JD. Curr Opin Struct Biol. 2008; 18:644–649. [PubMed: 19007887]

26. (a) Li C, Wu W, Kumar D, Shaik S. J Am Chem Soc. 2006; 128:394–395. [PubMed: 16402810] (b) Latifi R, Bagherzadeh M, de Visser SP. Chem Eur J. 2009; 15:6651–6662. [PubMed: 19472231] (c) Kumar D, Sastry GN, de Visser SP. Chem Eur J. 2011; 17:6196–6205. [PubMed: 21469227]

27. Jaguar 7.6. Schrödinger, LLC; New York NY: 2007. (b) Frisch, MJ.; Trunks, GW.; Schlegel, HB.; Scuseria, GE.; Robb, MA.; Cheeseman, JR.; Montgomery, JA., Jr; Vreven, T.; Kudin, KN.; Burant, JC., et al. Gaussian 03, revision C.02. Gaussian, Inc.; Wallingford, CT: 2004.

28. (a) Becke AD. J Chem Phys. 1993; 98:5648–5652.(b) Lee C, Yang W, Parr RG. Phys Rev B. 1988; 37:785–789.

29. (a) Kumar D, de Visser SP, Shaik S. Chem Eur J. 2005; 11:2825–2835. [PubMed: 15744771] (b) de Visser SP, Oh K, Han A-R, Nam W. Inorg Chem. 2007; 46:4632–4641. [PubMed: 17444641] (c) Vardhaman AK, Sastri CV, Kumar D, de Visser SP. Chem Commun. 2011; 47:11044–11046.

30. Hay PJ, Wadt WR. J Chem Phys. 1985; 82:270–283.

31. (a) de Visser SP. J Am Chem Soc. 2010; 132:1087–1097. [PubMed: 20041691] (b) Kumar D, Karamzadeh B, Sastry GN, de Visser SP. J Am Chem Soc. 2010; 132:7656–7667. [PubMed: 20481499]

32. (a) de Visser SP. Chem Eur J. 2006; 12:8168–8177. [PubMed: 16871510] (b) de Visser SP, Tahsini L, Nam W. Chem Eur J. 2009; 15:5577–5587. [PubMed: 19347895] (c) de Visser SP, Latifi R, Tahsini L, Nam W. Chem Asian J. 2011; 6:493–504. [PubMed: 21254427]

33. (a) Bassan A, Borowski T, Schofield CJ, Siegbahn PEM. Chem Eur J. 2006; 12:8835–8846. [PubMed: 16933342] (b) Lai W, Shaik S. J Am Chem Soc. 2011; 133:5444–5452. [PubMed: 21413763] (c) Latifi R, Tahsini L, Kumar D, Sastry GN, Nam W, de Visser SP. Chem Commun. 2011; 47:10674–10676.

34. Emerson JP, Farquhar ER, Que L Jr. Angew Chem Int Ed. 2007; 46:8553–8556.

35. (a) Rohde J-U, In J-H, Lim MH, Brennessel WW, Bukowski MR, Stubna A, Münck E, Nam W, Que L Jr. Science. 2003; 299:1037–1039. [PubMed: 12586936] (b) Martinho M, Banse F, Bartoli J-F, Mattioli TA, Battioni P, Horner O, Bourcier S, Girerd J-J. Inorg Chem. 2005; 44:9592–9596. [PubMed: 16323949] (c) Sastri CV, Seo MS, Park MJ, Kim KM, Nam W. Chem Commun. 2005; (11):1405–1407.(d) De Oliveira FT, Chanda A, Banerjee D, Shan X, Mondal S, Que L Jr, Bominaar EL, Münck E, Collins TJ. Science. 2007; 315:835–838. [PubMed: 17185561] (e) Jackson TA, Rohde J-U, Seo MS, Sastri CV, DeHont R, Stubna A, Ohta T, Kitagawa T, Münck E, Nam W, Que L Jr. J Am Chem Soc. 2008; 130:12394–12407. [PubMed: 18712873]

36. Riggs-Gelasco PJ, Price JC, Guyer RB, Brehm JH, Barr EW, Bollinger JM Jr, Krebs C. J Am Chem Soc. 2004; 126:8108–8109. [PubMed: 15225039]

37. (a) Kumar D, Hirao H, Que L Jr, Shaik S. J Am Chem Soc. 2005; 127:8026–8027. [PubMed: 15926822] (b) de Visser SP. J Am Chem Soc. 2006; 128:15809–15818. [PubMed: 17147391] (c) Hirao H, Que L Jr, Nam W, Shaik S. Chem Eur J. 2008; 14:1740–1756. [PubMed: 18186094] (d) Ye S, Neese F. Proc Natl Acad Sci USA. 2011; 108:1228–1233. [PubMed: 21220293]
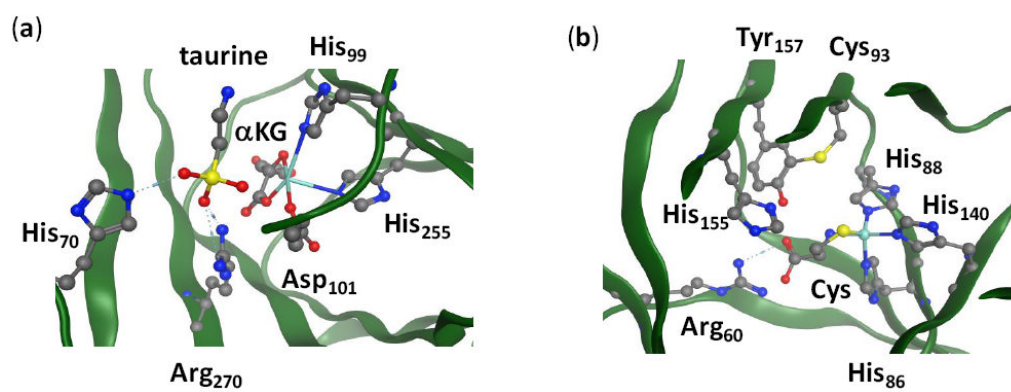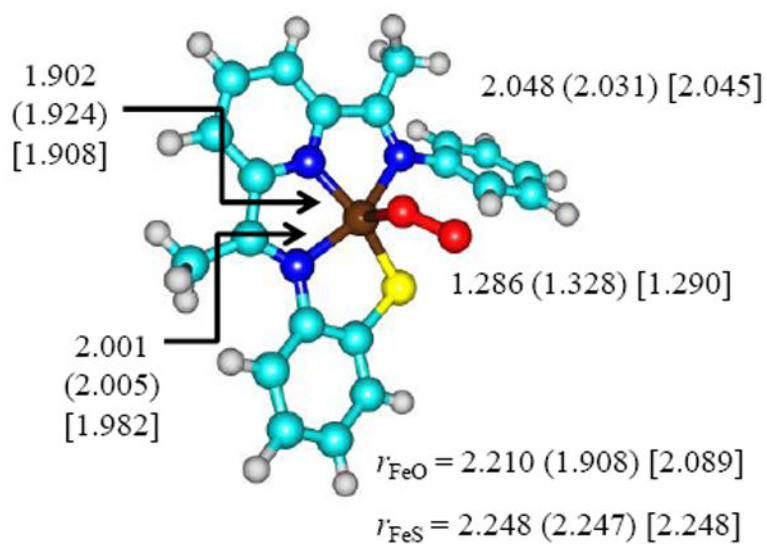
Figure 1.
The active sites of TauD (panel a) and CDO (panel b) as taken from the 1OS7 and 2IC1 pdb files. Amino acids are labeled as in the pdb files.

1.902
(1.924)
[1.908]

2.048 (2.031) [2.045]

2.001
(2.005)
[1.982]

1.286 (1.328) [1.290]

$r_{FeO} = 2.210\ (1.908)\ [2.089]$

$r_{FeS} = 2.248\ (2.247)\ [2.248]$

$\Delta E + ZPE(gas) = 2.1\ (8.2)\ [0.0]$
$\Delta E + ZPE(solv) = 1.4\ (5.5)\ [0.0]$
$\Delta G(gas) = -0.5\ (6.9)\ [0.0]$
$\Delta G(solv) = -1.2\ (4.2)\ [0.0]$

$^5A\ (^3A)\ [^1A]$

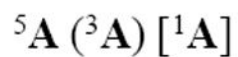**Figure 2.**
Optimized UB3LYP/BS1 geometries of ^{1,3,5}**A** with bond lengths in angstroms. Also given are relative energies in the gas-phase and relative free energies with values in kcal mol^{-1}.
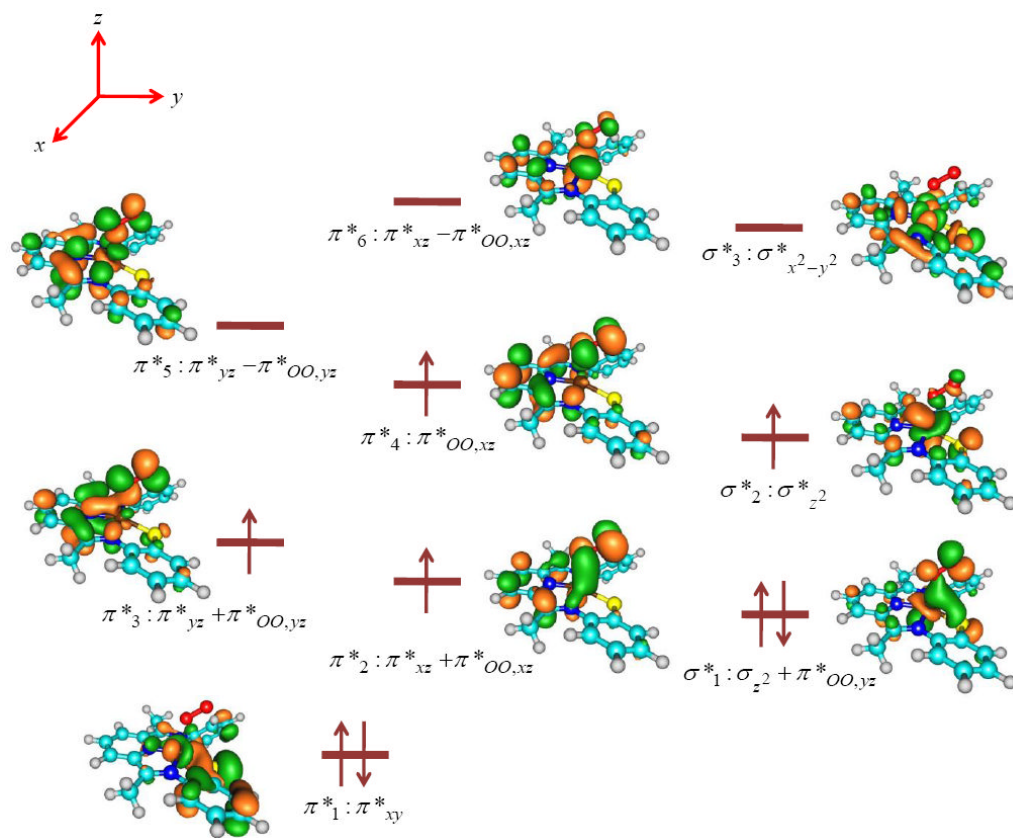
Figure 3.
High-lying occupied and low-lying virtual orbitals of ^{5}**A** as calculated with DFT methods. Orbital diagrams are taken from the β set of molecular orbitals.
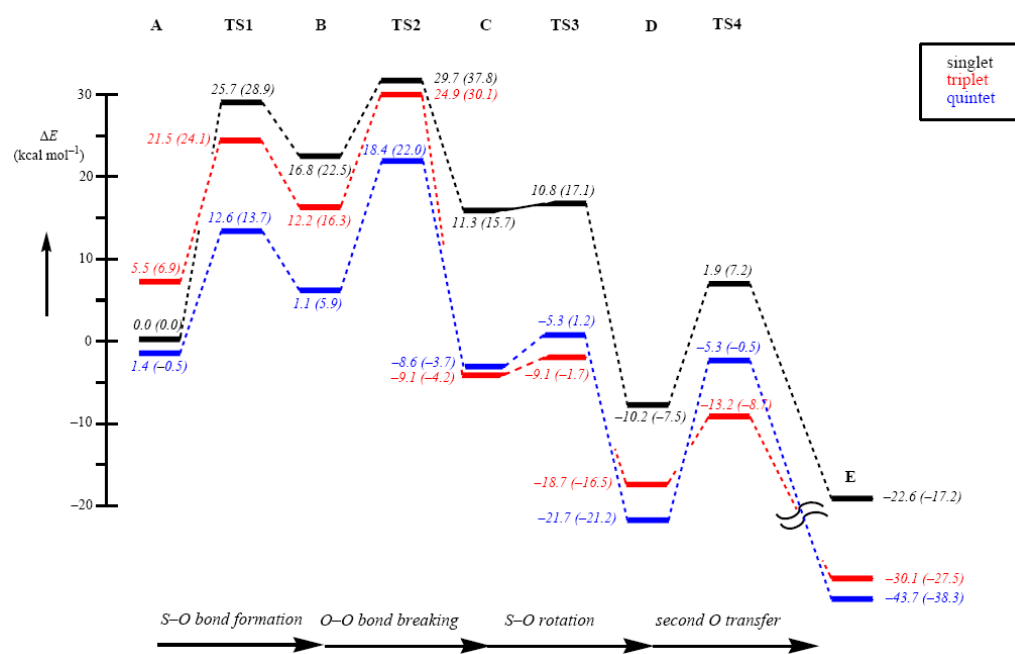
Figure 4.
Potential energy profile of oxygen transfer to the thiolate group of the LN_3S ligand starting from the $[Fe^{III}(LN_3S)O_2]^+$ complex. All energies are in kcal mol^{-1} relative to ^{1}**A**. Out of parenthesis are $\Delta E + ZPE + E_{solv}$ values and in parenthesis are free energies. The latter include entropic and thermal corrections at 298 K.
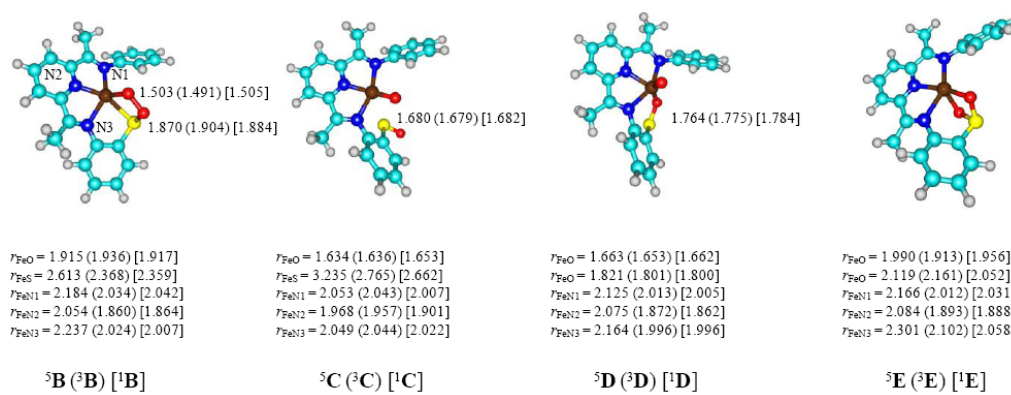
$r_{\text{FeO}} = 1.915\ (1.936)\ [1.917]$
$r_{\text{FeS}} = 2.613\ (2.368)\ [2.359]$
$r_{\text{FeN1}} = 2.184\ (2.034)\ [2.042]$
$r_{\text{FeN2}} = 2.054\ (1.860)\ [1.864]$
$r_{\text{FeN3}} = 2.237\ (2.024)\ [2.007]$

$^{5}\mathbf{B}\ (^{3}\mathbf{B})\ [^{1}\mathbf{B}]$

$r_{\text{FeO}} = 1.634\ (1.636)\ [1.653]$
$r_{\text{FeS}} = 3.235\ (2.765)\ [2.662]$
$r_{\text{FeN1}} = 2.053\ (2.043)\ [2.007]$
$r_{\text{FeN2}} = 1.968\ (1.957)\ [1.901]$
$r_{\text{FeN3}} = 2.049\ (2.044)\ [2.022]$

$^{5}\mathbf{C}\ (^{3}\mathbf{C})\ [^{1}\mathbf{C}]$

$r_{\text{FeO}} = 1.663\ (1.653)\ [1.662]$
$r_{\text{FeO}} = 1.821\ (1.801)\ [1.800]$
$r_{\text{FeN1}} = 2.125\ (2.013)\ [2.005]$
$r_{\text{FeN2}} = 2.075\ (1.872)\ [1.862]$
$r_{\text{FeN3}} = 2.164\ (1.996)\ [1.996]$

$^{5}\mathbf{D}\ (^{3}\mathbf{D})\ [^{1}\mathbf{D}]$

$r_{\text{FeO}} = 1.990\ (1.913)\ [1.956]$
$r_{\text{FeO}} = 2.119\ (2.161)\ [2.052]$
$r_{\text{FeN1}} = 2.166\ (2.012)\ [2.031]$
$r_{\text{FeN2}} = 2.084\ (1.893)\ [1.888]$
$r_{\text{FeN3}} = 2.301\ (2.102)\ [2.058]$

$^{5}\mathbf{E}\ (^{3}\mathbf{E})\ [^{1}\mathbf{E}]$

Figure 5.
Optimized UB3LYP/BS1 geometries of the critical points from Figure 3 with bond lengths in angstroms. Optimized geometries of $^{5,3,1}\mathbf{A}$ are given above in Figure 2.
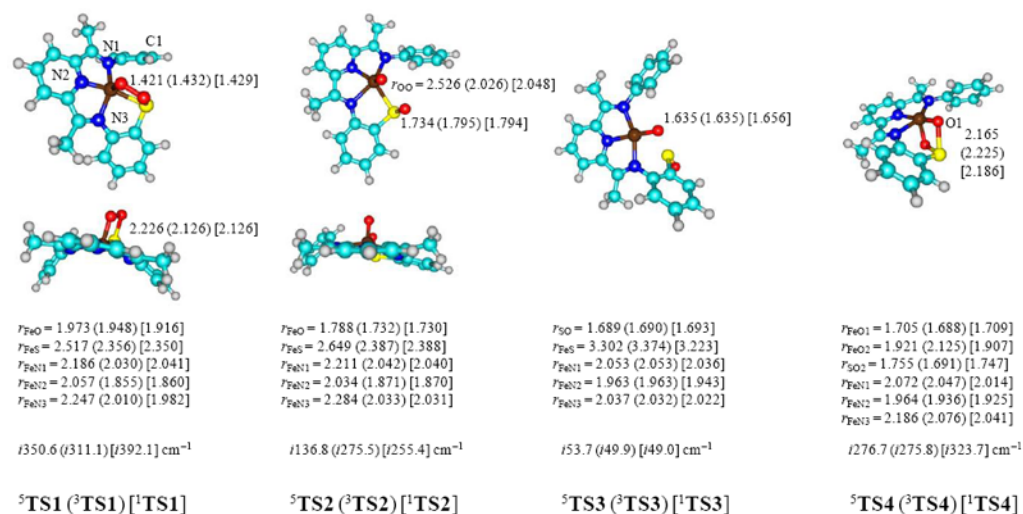
Figure 6.
Optimized UB3LYP/BS1 geometries of the transition states from Figure 4. Bond lengths are in angstroms and the imaginary frequency in the transition state in wave numbers.
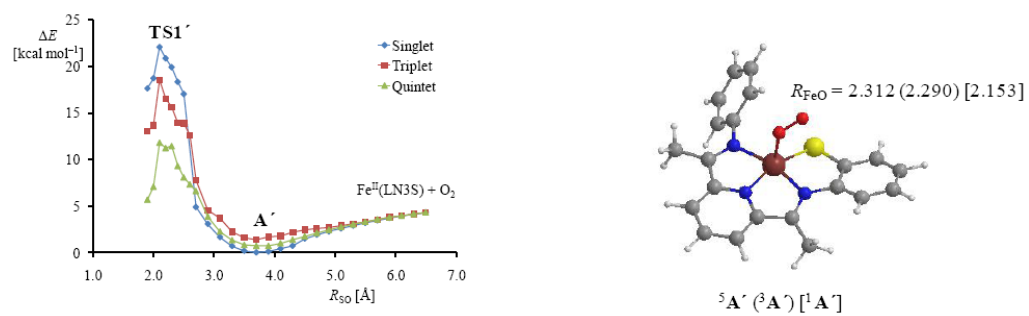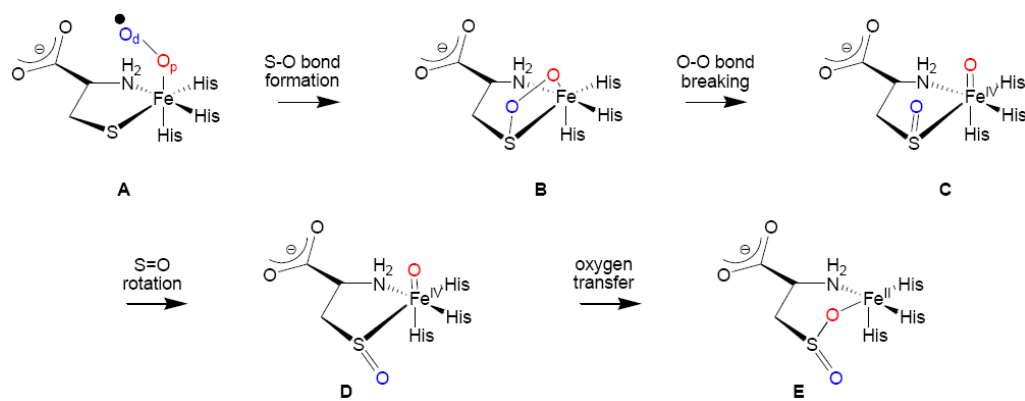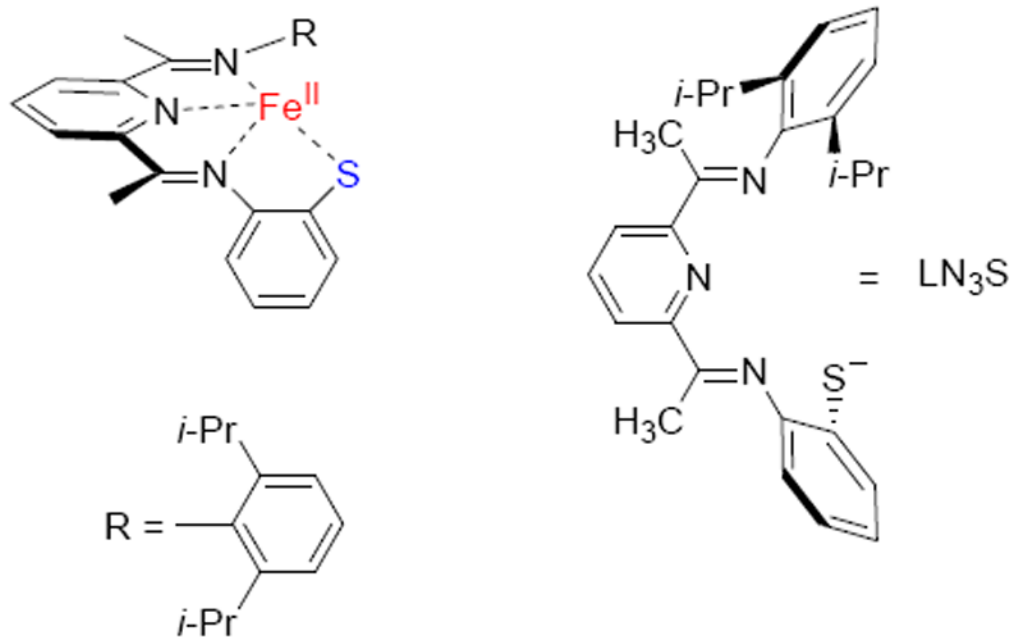
Figure 7.
Geometry scans for the approach of the dioxygen on the sulfur atom starting at a S–O distance of over 6 Å. Also shown is the geometry of the minimum point of the scan for the singlet, triplet and quintet spin states with the Fe–O distance (R_{FeO}) given in angstroms.

Scheme 1.
Dioxygen activation mechanism of CDO enzymes as established by computational studies.[12]

Scheme 2.
Biomimetic model of CDO.

Table 1

Relative energies of dioxygen transfer from iron(III)-superoxo to sulfur based substrate in (a) biomimetic CDO model, (b) CDO enzyme model as calculated using DFT model complex and (c) CDO enzyme model as calculated with QM/MM.

	$Fe^{III}O_2(LN3S)$	CDO Enzyme Model	
	DFT[a]	DFT[a,b]	QM/MM[c,d]
¹A	0.00	0.00	0.00
³A	5.51	2.01	5.80
⁵A	1.39	8.36	13.84
¹TS1	25.70	23.69	13.68
³TS1	21.53	25.39	24.19
⁵TS1	12.61	17.72	14.44
¹B	16.77	12.31	12.12
³B	12.20	10.26	10.88
⁵B	1.12	-0.42	2.87
¹TS2	29.75	29.08	14.93
³TS2	24.88	21.67	10.32
⁵TS2	18.41	5.92	5.75
¹C	11.27	9.33	-5.88
³C	-9.14	-9.85	-18.94
⁵C	-8.62	-8.54	-10.62
¹TS3	10.79	5.13	7.76
³TS3	-9.11	-4.66	-5.73
⁵TS3	-5.28	-5.29	-7.61
¹D	-10.23	-5.48	-9.87
³D	-18.67	-1.15	-19.02
⁵D	-21.66	-14.59	-18.73
¹TS4	1.93	1.70	-2.03
³TS4	-13.20	4.90	-1.31
⁵TS4	-5.32	-13.10	-12.58
¹E	-22.57	-26.10	-25.48
³E	-30.13	-32.88	-31.13
⁵E	-43.71	-40.72	-38.66

[a] ΔE+ZPE values with solvent corrections included.

[b] From Ref. 12b.

[c] ΔE+ZPE result.

[d] From Ref. 12c.